Contents list available at IJRED website

International Journal of Renewable Energy Development

Journal homepage: https://ijred.undip.ac.id

Research Article

Experimental Investigation of Bladeless Power Generator from Wind-induced Vibration

La Ode Ahmad Barata[1*], Kiwata Takahiro[2], Toshiyuki Ueno[2], Samhuddin[1], La Hasanudin[1]

[1]*Mechanical Engineering Department, Halu Oleo Univ., Kendari 93232, Indonesia*

[2]*Institue of Science and Engineering, Kanazawa Univ., Japan*

Abstract. The power harvester unit from flow-induced vibration (*FIV*) was designed to harness energy from low flow velocity based on the magnetostrictive effect on the galfenol (*Fe – Ga* alloy) strip induced by the oscillating bluff body. This study aimed to investigate the cross-section variation's effect on the *FIV* characteristics and the magnetostrictive material's performance for the bladeless power generator. The generator model's vibration characteristics and performance tests were conducted in the wind tunnel test using the wind-receiving unit (*WRU*) variation. The results showed that the resonance reduced-velocity (V_r) were around 3.7 and 4.0 for rectangular and circular cylinders, respectively. Furthermore, the effect of rectangular depth variation on the power generation output is linear to the test models' displacement rate and vibration frequency. The harvester's maximum power generation was 5.25 mW, achieved using the rectangular prism with depth $D = 0.4H$. The power coefficient was also evaluated for different wind-receiving models. The harvester model lit up 54 *LED* lamps in the wind tunnel test. The voltage output is sufficient to provide electric power resources for an *IoT* system, sensor, and wearable or wireless devices. The harvester model successfully generated a voltage signal under the initial field test with an ambient wind velocity of 0.9 – 2.71 m/s. Therefore, this study recommends the development of bladeless power generators in the future.

Keywords: Rectangular prism, Circular cylinder, Flow-induced vibration, Magnetostrictive material, Power generation, Power coefficient

Received: 4th Jan 2022; Revised: 7th April 2022; Accepted: 12th April 2022; Available online: 25th April 2022

1. Introduction

Recent innovative technology, such as the internet of things (*IoT*), wireless sensors, and microelectromechanical systems, necessitate independent power resources. In general, these systems require a low power supply that could be scavenged in the environment. Battery-based power connectivity has technical constraints such as leakage and recycling issues, electrical resistance, span life, and wire connectivity in confined places. Power supply sustainability for a pacemaker device implanted inside the human body, an onboard health tire system, elevated bridge, or structure monitoring leads to investigations on micropower resources. Mechanical vibration, human motion or organ beats, and fluid flow are some resources for the vibration-based power generators using piezoelectric or magnetostrictive-based material. Also, the undesirable mechanical vibration of the bridge structure, vehicle, and industries are interested in gaining power resources for instrumental devices. They aim to provide real-time monitoring data without batteries or recharging the battery. The investigation on vibration-based power generator found that a micro electric power supply cannot be granted conventionally, such as a pacemaker using heartbeat and onboard health tire monitoring system embedded in vehicle part (Poloni and Lu, 2017; Alrashdan, Hamzah, and Majlis, 2015; Ansari and Karami, 2015; Matsuzaki and Todoroki, 2008). Yan *et al.* (2018) and Romero-Ramirez (2010) examined a vibration-based power model to gain the potential power resources from the human body. Many studies on vibration-based micropower harvesters use intelligent materials such as piezoelectric. However, power generation based on magnetostrictive material has also been developed recently.

The magnetostrictive material for harnessing energy systems was evaluated by Liu *et al.*(2020), Apicella *et al.* (2019), Liu *et al.* (2019), Narita and Fox (2018), Anton and Sodano (2007), and Mitcheson et al. (2004). The electric voltage could be gained from a harmonic displacement of prismatic structures using a magnetostrictive material as the micropower harvester with a bladeless vortex generator model. This method is considered convenient in evaluating the harvester's performance. Smart materials such as *galfenol* (iron-gallium alloy) and *terfanol* for the micropower generation core have outstanding features.

* Corresponding author:
Email: ahmad.barata@uho.ac.id (L.O.A. Barata)

https://doi.org/10.14710/ijred.2022.43888
ISSN: 2252-4940/© 2022.The Author(s). Published by CBIORE

These include excellent machinability, good mechanical properties, suitable for high-frequency vibration, and high inverse magnetostrictive (Mohanty *et al.*, 2019; Ahmed *et al.*, 2017; Ueno and Yamada, 2011; Wang and Yuan, 2008). The *WRU* aerodynamics is an essential parameter for power generation from *FIV* in developing a bladeless power generator.

Studies have examined the flow dynamic response or aerodynamic/hydrodynamics aspects of the performance of vibration-based power harvesters. For instance, Derakhshandeh *et al.* (2015), Abdelkefi *et al.* (2016), and Bernitsas *et al.* (2008) examined harvesting energy from flow-induced motion with vortex-induced vibration and galloping with various modes. Galloping and vortex excitation vibration characteristics modes improve electricity voltage gained from *FIV* by defining certain bluff bodies (Wang *et al.,* 2020). However, bluff body configuration did not consider the effect of flow behavior in the after-body on the dynamic response of bluff bodies. Power generation improvement is proportional to the vibration displacement magnitude and the rate of vibration frequency. They are closely related to the flow pattern around the cylinders, suggesting that the power harvester performance depends on *WRU* characteristics. Therefore, improving the dynamic response of bluff bodies enhances the harvester's voltage output and enables gaining power in low flow velocity. The vibration frequency and displacement characteristics are determined by aerodynamic or hydrodynamics of the bluff body and damping system. The classical investigations of these phenomena were conducted by Nakamura and Hirata (1991), Zdravkovich (1981), Bearman (1984), and Blevins (1974). Moreover, Barata *et al.* (2020), Zhong *et al.*(2019), and Kiwata *et al.* (2014) examined the effect of span length and depth variation on the rectangular prism displacement in the water tunnel test.

Okajima and Kiwata (2019), Sumner *et al.* (2017), Mizukami *et al.*(2017), and Rostamy *et al.* (2012) examined the flow structure around a prismatic structure with an end tip effect. The three-dimensionality of flow structure affects dynamic response characteristics such as the bluff body's initial and magnitude vibration. Direct application of vibration-based power generation to the environment needs a well-designed wind receiver. Therefore, it is essential to implement a suitable *WRU* for the harvester energy systems to gain optimum power generation in the low wind velocity. The ambient vibration could be a sustainable power resource for an intelligent sensor, wearable, wireless, or confined devices, and health monitoring of elevated structures. The vibration response characteristics of *WRU* are the primary consideration for selecting an appropriate bluff body model. The designed bluff body could be the prospective model for the harvester energy from *FIV,* which is reliable for sensor and wearable or wireless device power resources. Therefore, this study examined the vibration mechanisms of a circular cylinder and rectangular prism bluff bodies.

This study aimed to investigate the effect of depth variation of the rectangular and circular cylinders on the vibration response characteristics of the test models. It also aimed to examine the performance of a power generator from wind-induced vibration.

1.1 Wind-induced Vibration

The vibration power generator concept works on fluid-structure interaction (*FSI*) of vortex excitation or galloping modes coupled to the energy harvester. Vortex excitation at circular and square cylinders occurs when frequency characteristics match vortex-shedding frequency. The dynamic response of the rectangular prismatic bluff body below the critical depth ($D < 0.6H$) is induced by the instability of vortices around the prism related to the negative fluid force. This vibration is not vortex-induced and not related to vortex shedding frequency. However, high resonance occurs when vortex-shedding frequency shifts to the cylinder's characteristics or natural frequency (Bearman, 1984; Nakamura and Hirata, 1989; Williamson and Govardan 2004).

One vibration characteristic quantity is the resonance reduced-velocity (V_r), which is the non-dimensional velocity shown in equation (1). The cylinder's frequency characteristic (f_c) is approximated as the test model's natural frequency.

$$V_r = \frac{U_\infty}{f_c \cdot H} = \frac{1}{St} \quad (1)$$

Where U_∞ and St represent flow velocity and non-dimensional vortex shedding frequency, respectively.

The transverse displacement velocity for bending type displacement is varied along the *WRU* span. Therefore, the beam deflection unit angle is approximated using the displacement rate at the defined measurement point of the *WRU* written as equation (2).

$$\theta_{rms} = \frac{y_{rms}}{L} \times \frac{180}{\pi} \quad (2)$$

Where y_{rms} is the root mean square of transverse displacement unit at measurement point L^*, while L is the total length of receiving unit and beam length to the center of bending.

1.2 Power Generation from Flow-induced Vibration (FIV)

A simple vibration generator is a bending model energy harvester where a galfenol sheet as a core is wounded by some turning coils. Voltage is generated by magnetic flux density variation during the core's dynamic motion. The magnetic field orientation is changed to produce a potential voltage, as shown in Fig. 1(a). The voltage generation (V) is proportional to the dynamic frequency (f_s), core area (A), and magnetic flux density variation (B). The last term is an inherent galfenol core property presented by Jafari *et al.* (2017); Mohammadi and Esfariandi (2015) as equation (3).

$$B = d^* \sigma + \mu^\sigma H \quad (3)$$

The intensity of this quantity is linear to electric potential difference generated by cantilevered type-bending harvester is shown in equation (4).

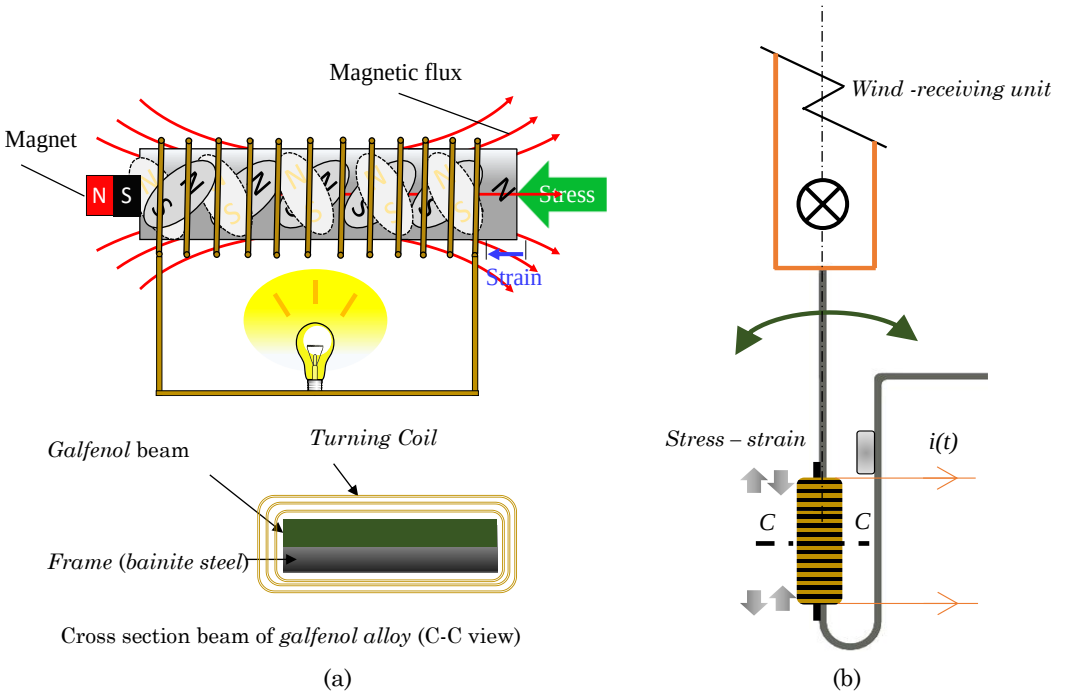

Fig. 1. (a) Inverse magnetostrictive effect on galfenol, (b) The schematic diagram of bending type galfenol (*Fe – Ga* alloy) based-power generator with cantilevered *WRU*

$$V(t) = 2\pi f_s BA \tag{4}$$

Where B is magnetic flux, d^* is flux variation with stress (σ) at constant H, μ^σ is magnetic permeability at constant σ, and H ($= N \times i/l$), N, i, and l is the number of coil turns, induce current and core length, respectively.

The harvester's power generation is given by:

$$P_{rms} = \frac{V_{rms}^2}{R} \tag{5}$$

Where R is the turning coil's resistance.

Since the harvester beam is cantilevered coupled to the *WRU*, the galfenol-based power generator efficiency is defined by the root mean square (*RMS*) of the generator power coefficient (*C.P.*). This is a power ratio extracted by the harvester over the fluid power transferred to the system.

$$C.P = \frac{P_{rms}}{0.5 \times \rho_f \cdot U^3 \left(\frac{\theta_{rms}}{360} \times L \right)} \tag{6}$$

Where $((\theta_{rms}/360)\times L)$ is swept area of the cantilevered-type bluff body, y, H, ρ_f, is displacement rate at measurement point L^*, cross-section height of the receiving unit, and air density, respectively. The denominator of equation (6) is fluid kinetic energy quantity derived from the Bernoulli equation.

Betz (1966) introduced the optimal power extracted by energy harvester 16/27 of ideal efficiency because not all fluid energy could be converted by the harvester. The power generated by the harvester unit is calculated by multiplying the fluid kinetic term in equation (6) by Betz's coefficient in equation (7).

$$C.P_{\max} = \frac{P_{rms}}{E_{fluid} \cdot \left(\frac{16}{27} \right)} \tag{7}$$

2. Experimental Approach

2.1 Conceptual design of the wind-receiving unit (WRU)

The power harvester is expected to harness energy in various flow regimes, low vibration onset, and high efficiency, with reliable performance during intense winds. The dynamic response is essential for extracting optimum flow kinetic energy. *WRU* is designed based on vibration characteristics of rectangular prism developed by Nakamura and Hirata (1991). Moreover, vortex-induced motion characteristics studies on the circular cylinder introduced by Williamson and Govardhan (2004), Blevins (1974), Bearman (2011) are considered. This study employed a finite *WRU* length with cantilevered type using the rectangular and circular test models. Table 1 shows the physical properties of the *WRU* models.

The WRU test models were constructed using the 3D print *RAISED3D Inc.* and *N2S Plus* with *RAISED3D Premium PLA* resin filament, as shown in Fig. 2(b). The test models have a constant cross-section height (H) and diameter (D) of 40 mm, span lengths (L) of 200, 300, and 400 mm, and different mass ratios (M).

Table 1
Physical properties of *WRUs*

Length	Circular (D = H=1.0)			Square (D =1.0H)			Rectangular (D = 0.5H)		
L[mm]	f_c[Hz]	C_n	M	f_c[Hz]	C_n	M	f_c[Hz]	C_n	M
200	14.8	3.9	42.3	12.2	3.8	46.4	15.0	6.4	78.1
300	8.5	3.0	36.3	7.4	5.3	40.3	9.5	9.5	67.4
400	6.0	3.9	32.9	5.2	4.3	36.8	6.4	6.2	65.1
	Rectangular (D = 0.4H)			Rectangular (D = 0.3H)			Rectangular (D = 0.2H)		
L[mm]	f_c[Hz]	C_n	M	f_c[Hz]	C_n	M	f_c[Hz]	C_n	M
200	16.6	13.1	70.7	15.4	11.2	90.0	17.6	17.4	124.0
300	10.1	6.6	61.2	9.3	11.2	73.5	11.0	7.1	111.7
400	6.7	5.3	57.8	6.6	6.4	71.5	7.4	8.5	105.3

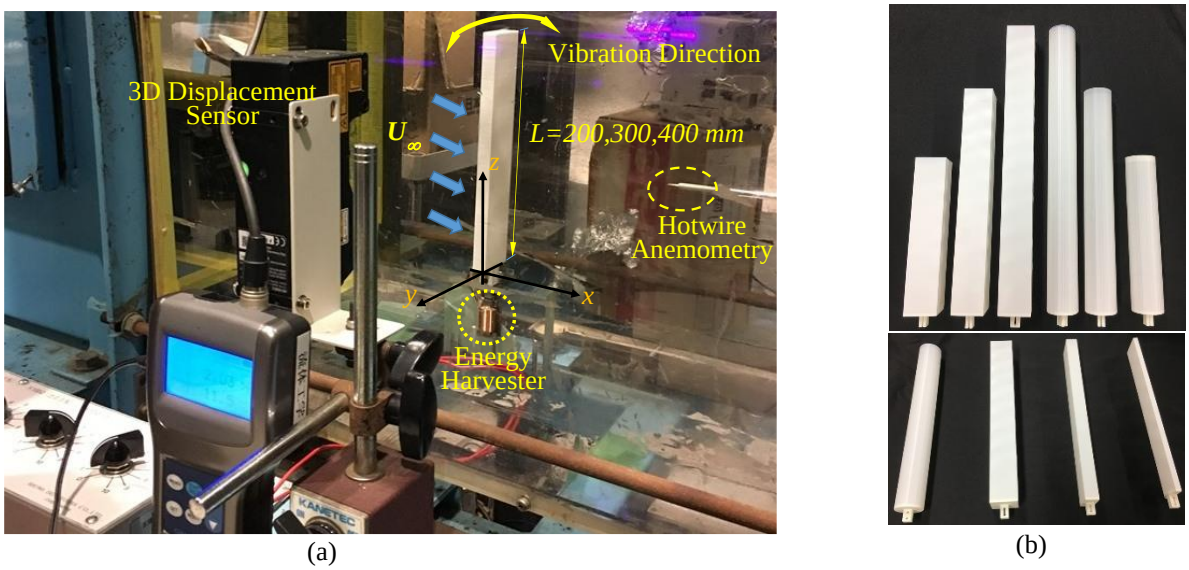

Fig. 2. (a) Test section of the wind tunnel, (b) Cross-section of square and circular cylinders test model with different aspect ratios (top) and the test model of rectangular prisms with side ratios of 0.2 and 0.5, square and circular cylinder with constant span length (bottom).

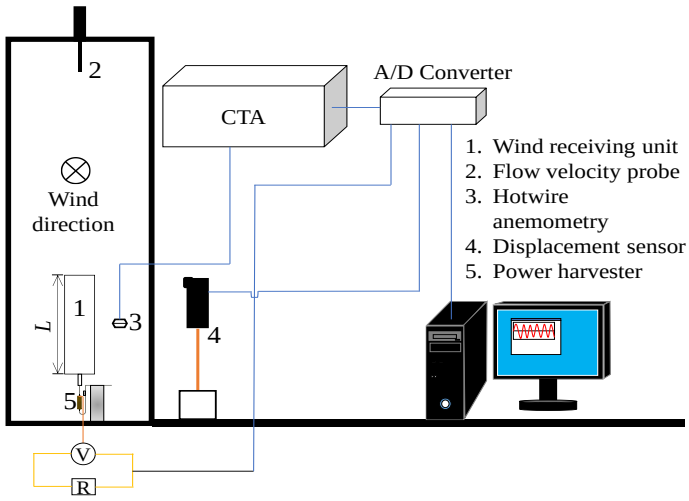

Fig. 3. The Schematic diagram of *FIV* and power generation tests

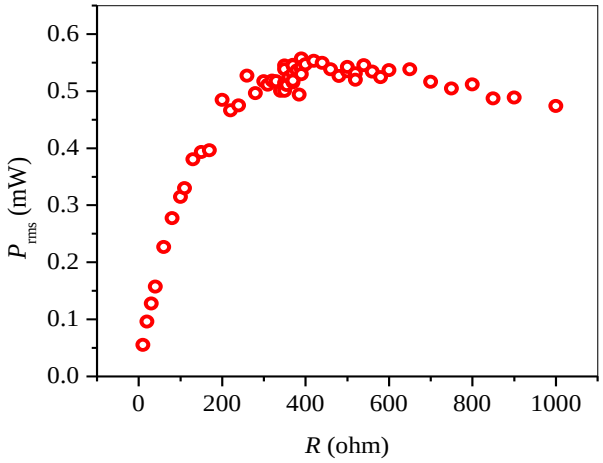

Fig. 4. Optimum resistance of the energy harvester

2.2 Power generation

The energy generation and *FIV* tests were performed simultaneously in a wind tunnel test section of 30×2000×1200 mm. The vibration-based generator was constructed from a *galfenol* ($Fe_{81.6}Ga_{18.4}$) of 8×26×1 mm alloy wounded by a 0.1 mm induction wire with 5627 turns. Moreover, a permanent magnet of *neodymium* of 6×12×1.5 mm was mounted to a frame made from *bainite* steel with 1 mm in thickness. The vibrator and harvester energy was coupled mechanically using a bolt and allowed to vibrate in the transverse direction. The schematic of the experimental arrangement and the power generation test are shown in Figs. 2(a) and 3, respectively. The prism's effective mass influences the test model's frequency characteristics (f_c). The reduced mass damping parameter C_n (= 2*δ*M, where δ is the decay rate of prism amplitude obtained by exerting manual trigger at stationary flow, M is the ratio of a structure's effective mass to air mass at atmosphere state). The displacement rate of the *WRU* was obtained using a three-dimensional laser beam displacement sensor (*KENYENCE, LJ-V7200*). Furthermore, the flow stream fluctuation was measured using a cylindrical straight probe *0251R-T5 KANOMAX*. The output signals were transferred to an integrator 14-bit A/D converter analog with a sampling frequency of 2 kHz, and 16,834 data points were stored.

Flow stream rate was measured using a tube anemometer (*KANOMAX Climomaster Anemometer 6501 Series, 6541-21*). The velocity of the flow stream was varied from 0.9 to 6.0 m/s with Reynold number Re = ($U_\infty H/\nu$) of 2.4 ×10^4 to 1.6 ×10^5 by changing the fan's motor frequency input. The power generation P (=V_{rms}^2/R) was calculated from the rated power voltage output of the signal converter. All instruments were calibrated according to the standard before performing the *FIV* and energy harvesting experiment. Also, the generator's variable resistance at constant flow stream velocity was examined before the experiment to determine the micro harvester's optimum resistance (R). Fig. 4 shows that the harvester's optimum resistance is 370 ohm and was employed for the power generation test.

The power generation principle is based on the inverse *magnetostrictive* phenomenon where the oscillation of the wind receiving structure bends the *galfenol* beam, resulting in a magnetic flux change. Electromotive force for the time oscillation drives the electrical circuit through a permanent magnet. The power conversion is based on Faraday's law that winding induction coil produces a potential difference through electromagnetic force, as shown in Fig. 1(a).

3. Results and Discussion

3.1 Vibration response of the test models

Figs. 5 and 6 show the displacement rate of the rectangular prisms for resonance reduced-velocity. The test models exhibited similar onset vibration at the resonance reduced-velocity V_r around 3.8 except for a square prism. The rectangular prism galloping is similar to the range defined by Nakamura and Hirata (1991). However, the critical reduced-velocity V_{rcr} value is higher than that defined by Nakamura and Matsukawa (1987). For span length L = 5.0 H, there were no abrupt vibration response changes for flow velocity (U) less than 5.0 m/s or V_r < 7.0. In this case, flow velocity did not reach the designed range due to experimental apparatus and test model limitations. The rectangular prisms with span lengths L = 7.5 and 10H showed declining displacement at critical resonance velocity. Table 2 shows the critical resonance reduced-velocities. The displacement rate vanished after reaching the critical resonance reduced-velocity for the prisms with $D \leq 0.4H$. However, a second galloping mode was observed at $D = 0.4H$ till the response vanished at V_r = 12 and 13 for prisms with span length L = 5.0H and 10H, respectively. Additionally, a second galloping mode was observed at the prisms with $D \geq 0.5H$.

The critical resonance reduced-velocity V_{rcr} of the rectangular prism is lower than that of the infinite prism (Table 2). The spanwise and tip end vortex effect alters the flow pattern in the wake related to the dynamic response of the elastically mounted prism (Gonclaves, 2015; Okajima, 1998; Sakamoto, 1985). The vibration response mechanism for side ratios $0.2 \leq D/H \leq 0.4$ are similar according to Nakamura and Hirata (1989) and Okajima (1982). The dynamic response of the rectangular prisms with depth below critical depth $D \leq 0.4H$ is the instability vibration or shear layer separation at the leading edge that creates unstable aerodynamics forces around the prism.

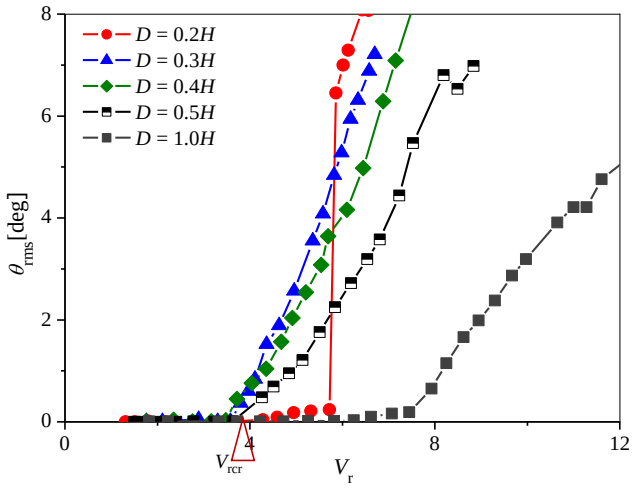

(a) Span-length L = 5 H

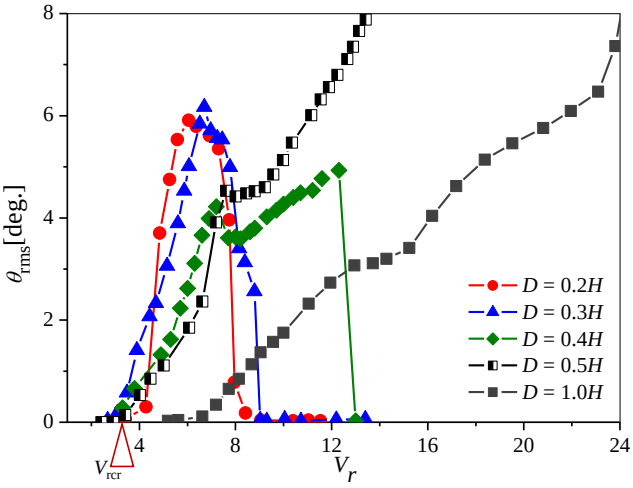

(b) Span-length L = 7.5 H

Fig. 5. Response amplitude of the rectangular prisms versus non-dimensional velocity

Table 2
The critical resonance reduced-velocity of oscillated rectangular prisms

Finite length	D/H			
	0.2	0.3	0.4	0.5
L/H	V_{rcr} (U)	V_{rcr} (U)	V_{rcr} (U)	V_{rcr} (U)
5	5.7 (4.0)	3.8 (2.3)	3.7(2.5)	4.2(2.5)
7.5	4.3 (1.9)	3.5 (1.2)	3.5(1.4)	4.0(1.5)
10	3.5(1.1)	4.0(0.95)	3.3 (0.9)	4.2(1.0)
Infinite Length(*)	7.3	7.5	7.8	8.0

(*) Nakaguchi, *et al.,* 1968, and Okajima *et al.*,1998

The response is determined by minus lift force component versus attack angle. The displacement response increased linearly by uptick flow stream velocity, but the prism with depth D = 0.2H exhibited a sudden jump at the V_r of 5.86. This test model showed the highest vibration frequency. Additionally, no hysteresis occurred for all test models when flow stream velocity was reduced regularly during the experiment.

The initial vibration of prisms with span length L = 7.5 and 10H against flow velocity are lower than span length L = 5.0H. However, they have similar onset galloping against resonance reduced-velocity because of their difference in frequency characteristics. The rectangular prism with depth $D \leq 0.5H$ exhibited similar onset galloping at resonance reduced-velocity V_r = 3.7 for all span lengths. The onset galloping varies against flow velocity due to variation of the natural frequency of the prism. The prisms below critical depth $D < 0.6H$ have similar flow feature characteristics. Furthermore, flow feature alteration is considered at the prisms with $D \geq 0.6H$ closely related to vibration response characteristics (Nakamura and Hirata, 1991; Nakamura and Matsukawa, 1987)

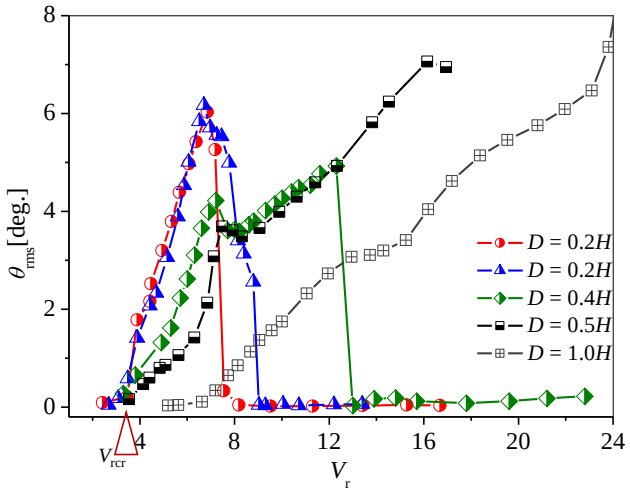

Fig. 6. Response amplitude of rectangular prisms for non-dimensional velocity for a span-length $L = 10H$

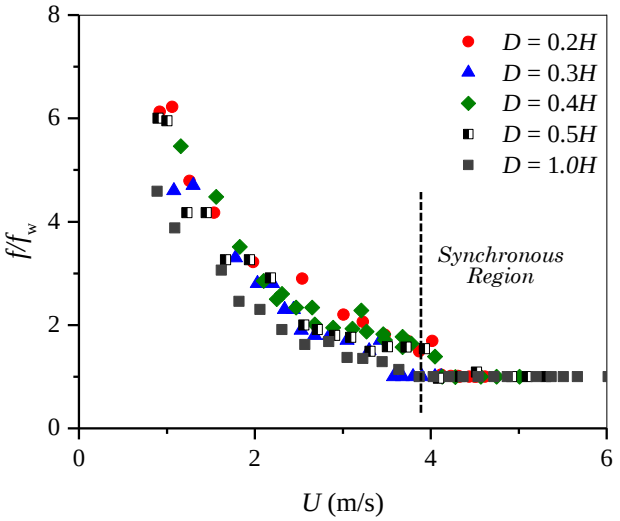

Fig. 7. The normalized vibration frequency of the prism test models with a span length $L = 5H$.

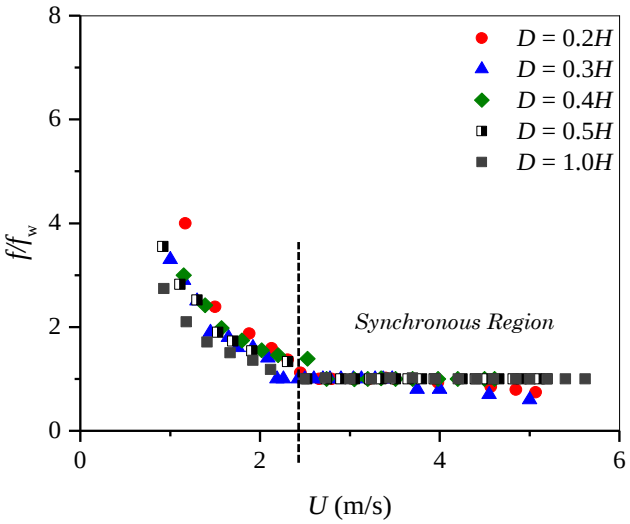

Fig. 8. The normalized vibration frequency of the prism test models with a span length $L = 7.5H$

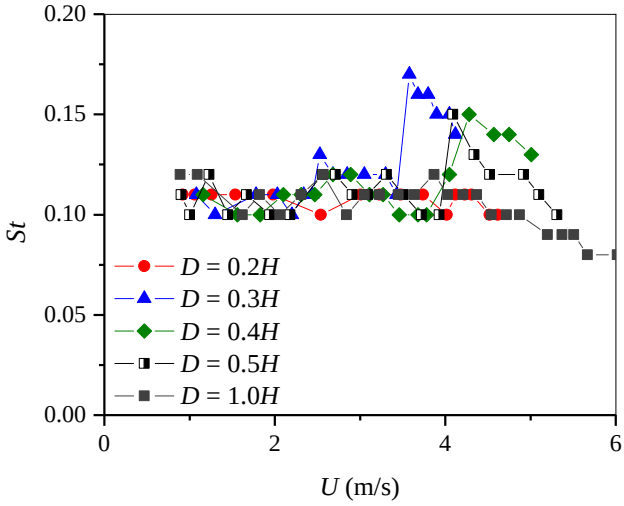

Fig. 9. Non-dimensional vortex shedding frequency of the prism test models with a span length $L = 5H$.

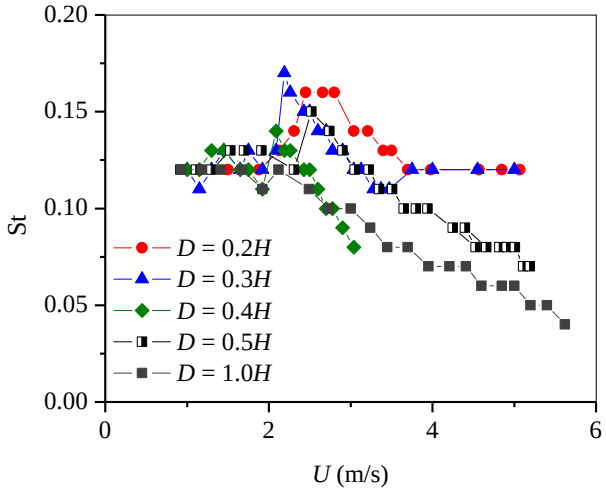

Fig. 10. Non-dimensional vortex shedding frequency of the rectangular prism for flow velocity for a span length $L = 7.5H$

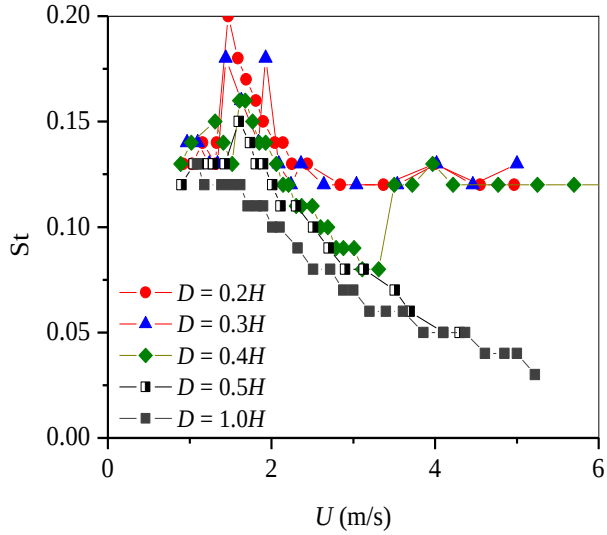

Fig. 11. Non-dimensional vortex shedding frequency of the rectangular prisms for flow velocity for a span-length $L = 10H$

Figs. 7 and 8 show normalized vibration frequency for flow velocity variation. Vortex shedding is low at a low-velocity stream and increases with the flow velocity. However, the vibration onset of the prisms with depth (D) below the critical depth is independent of vortex shedding frequency. This is a prominent feature of instability type vibration where the normalized frequency is greater than 1 at initial galloping. It is a different mechanism to the square prism that the natural and vortex-shedding frequencies must be equal to initiate vibration. High resonance occurs at the vortex resonance for prisms below the critical depth, where the cylinder frequency characteristic approach vortex frequency ($f_c/f_w \approx 1$). It is initiated at $U \approx 4.0$ for prisms with a span length of 200 mm. All prisms with a span length of 300 mm experienced a synchronization region at $U = 2.6$ m/s, after which the normalized frequency was less than 1.0 because vortex-shedding frequency developed continuously. Figs. 9, 10, and 11 represent non-dimensional vortex-shedding frequency for flow velocity. A non-dimensional vortex- shedding frequency jumped when the prisms started vibrating because wake frequency synchronizes to vibration response. A square prism showed a small jumping of non-dimensional vortex shedding because it has low-frequency characteristics but an extensive vibration range. When the vibration response diminished at flow velocity U_∞>3.0 m/s, non-dimensional vortex shedding variation was constant, except for prisms with a span length of 200 mm

Fig. 12 shows the vibration response of the circular cylinder against resonance reduced-velocity. In this case, the vortex resonance depends on the wake shedding frequency variation. The vibration response for a circular cylinder started when the wake frequency matched the natural frequency of the cylinder as the square prism. However, the vibration response characteristic and the critical resonance velocity of a circular cylinder are different and less than the square prism, respectively.

At high V_r, the circular cylinder experienced descending response as the rectangular prism with depth D<0.5H, but different to the square prism. Flow separation is fixed at the leading edge for rectangular prisms, and a separated shear layer development depends on the depth. The separation point is different from a circular cylinder because the wake flow pattern is altered at high flow velocity (Bearman, 2011; Palau-Salvador *et al.*, 2010; Wang and Zhou 2009; and Williamson and Govardan, 2004). Fig. 13 shows vortex-shedding frequency jumped to around 0.23 when the synchronous region occurred at the onset of galloping. The frequency then descended until the synchronous region was surpassed, and the response vibration vanished. The Strouhal frequency of the finite circular cylinder with different span lengths is typical around 0.17 at a high velocity where vibration response diminishes.

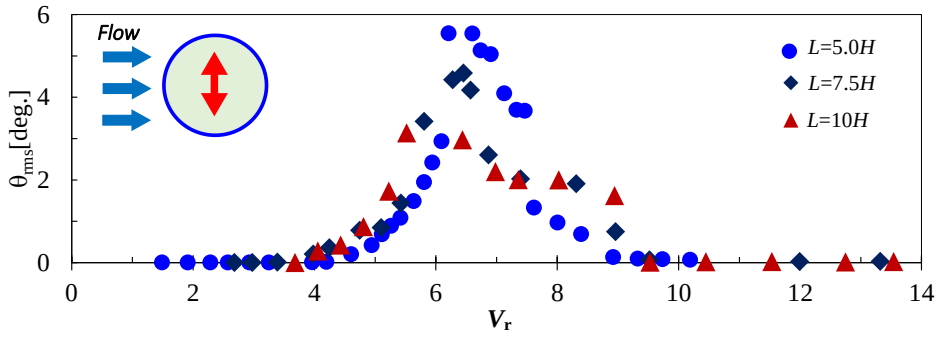

Fig. 12. Response amplitude of circular cylinder

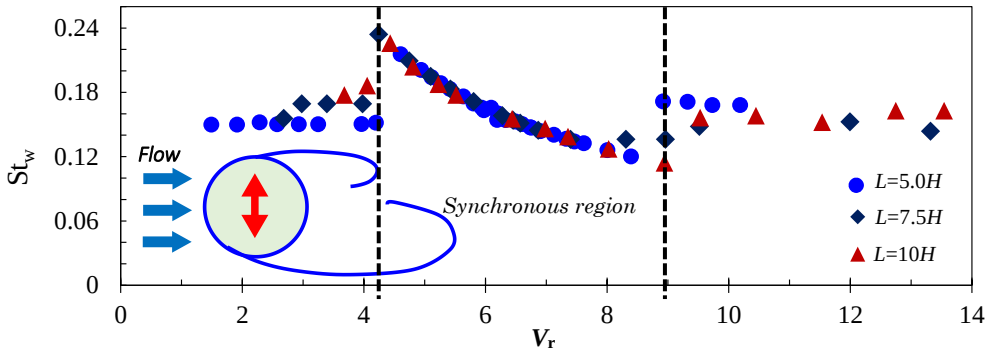

Fig. 13. Non-dimensional vortex-shedding frequency of circular cylinder

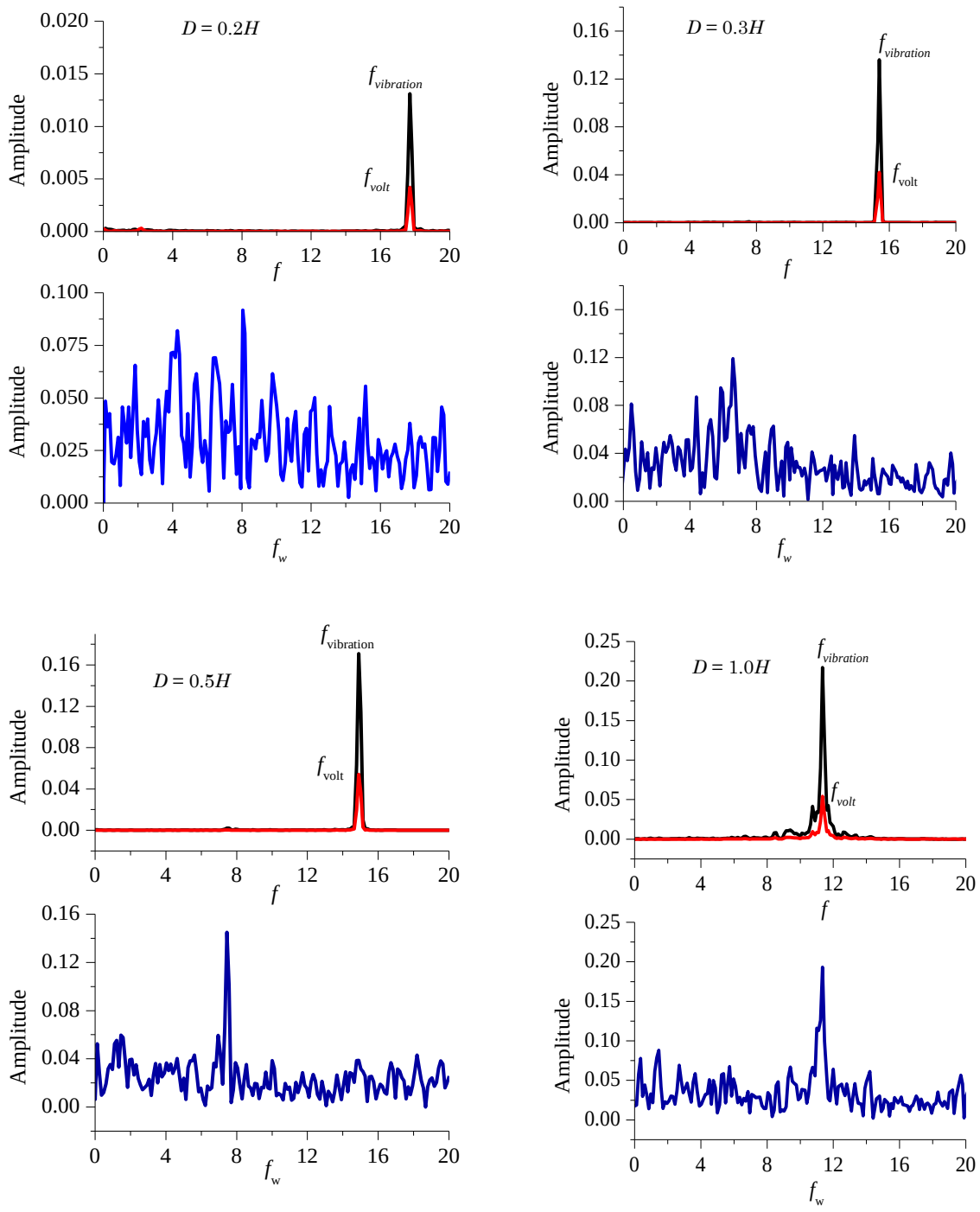

Fig. 14. Frequency response of the rectangular prisms test with length of 200 mm at onset galloping (displacement rate y_{rms} > 1 mm)

Fig. 14 presents the *FFT* frequency analysis of the rectangular prisms with depth variations for vibration response frequency, voltage, and wake. The prism with depth $D < 0.5H$ showed that frequency response does not match wake frequency, except the square prism. The fluctuation of wake diminishes by increasing the prism's depth, though the rectangular prisms showed only one sharp peak on the *FFT* spectra. Minor peaks adjacent to the sharp peak on the *FFT* spectra appear at a square prism, indicating a lag vibration response due to friction (Ohya, 1994). The vibration and voltage frequency signals are synchronous because they were coupled mechanically in the experimental setup. Additionally, vortex-shedding fluctuation at the trailing edge descended by increasing the prism's depth, as shown in Fig. 14. In contrast, the peak spectra matched the natural frequency of the square prism at initial galloping.

3.2. Power generation test

Power output coincides with the wind-receiver unit's displacement and frequency. The relation of these parameters to power generation output is their quadratic. Fig. 15 presents the harvester's *RMS* power output with various *WRU,* showing that reducing the displacement frequency is concomitant with power output decline. The rectangular prism test models with the length of 200 mm did not exhibit abrupt power generation decline because it has a short flow velocity range for power harvesting. The harvester system's capacity of vibration response is a shortcoming in harnessing energy using this model due to high resonance at maximum flow velocity. Span length variation affects frequency response and power generation output in this case. However, the displacement rate is similar to the test model with a span-length $L = 7.5H$, as shown in Fig. 15(b). Power harvesting characteristic is similar to response amplitude characteristics for depth variation of the rectangular prism. Furthermore, the prism's depth variation for a similar span length affects the prism's effective mass and vibration frequency response, reducing the generator's power output rate. This is consistent with Ueno and Yamada (2011) and Apicella *et al.* (2019), which used a galfenol (*Fe-Ga*) strip for the energy harvester.

Fig. 16(a), (b), and (c) show the power harvester's performance under *WRU* variations for span lengths of 200, 300, and 400 mm, respectively. The receiving unit's displacement response development is linear to the harvester's power generation. The generator achieved an *RMS* maximum of power generation of 5.25 mW at V_r = 3.26 (5.01 m/s) using the *WRU* with a depth of $D = 0.4H$. However, the power coefficient was slightly lower than the prisms with depth $D < 0.4H$. This test model shows the wide flow velocity power harvesting range. Increasing the rectangular prism depth decreased the harvester's performance, but the displacement rate of *WRU* remained unchanged. The *RMS* power generation rate for the circular cylinder test model was achieved at low flow velocity.

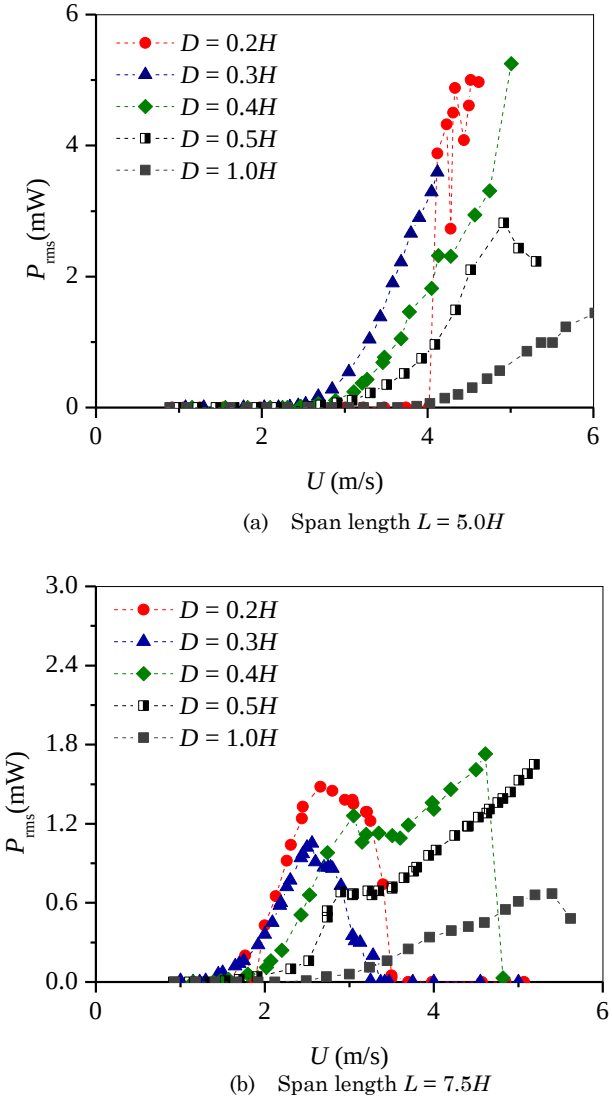

(a) Span length $L = 5.0H$

(b) Span length $L = 7.5H$

Fig. 15. *RMS* power output of the harvester energy for rectangular prism with span length

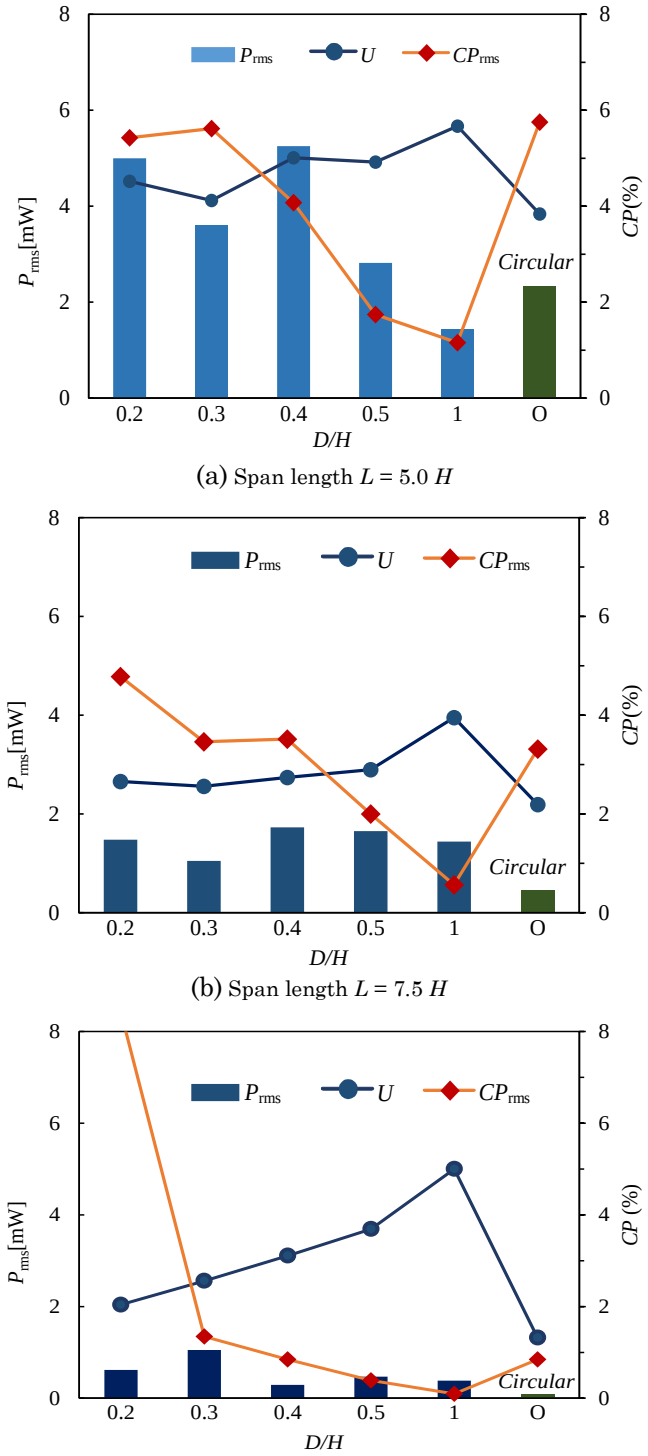

Fig. 16. The performance of power harvester for various *WRU*

Although its peak performance is better than the rectangular prisms, it has lower *RMS* power generation. Kiwata et al. (2013) examined an *FIV*-based power generator in a water tunnel using a cantilevered rectangular prism with $D = 0.2H$ and a higher frequency characteristic than the present model. The model generated 8.8 mW at resonance reduced-velocity V_r about 5.0.

The test models with depth $D < 0.4H$ exhibited a limited power harvesting range different from depth $D \geq 0.4H$ with an extensive power harvesting range. The generator gained high *RMS* peak power generation but lower power efficiency than the rectangular test model with depth, $D = 0.2H$. Moreover, the generator achieved the highest peak performance using a rectangular prism with depth $D = 0.2H$ because the *RMS* peak of power generation is achieved at low flow velocity.

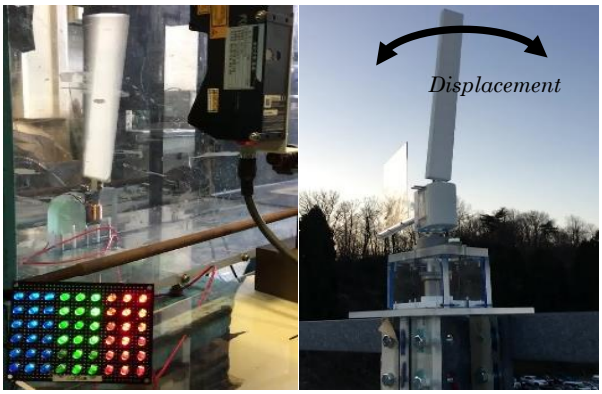

(a) (b)

Fig. 17. Bladeless power generator performance test (a) in wind tunnel test with a flow velocity of 3.25 m/s, (b) Initial field test

The lowest *RMS* power generation of less than 1.0 mW was found at the generator using a circular *WRU*. Increasing the span length of *WRU* from $L = 5.0H$ to $L = 10H$ reduced a double of vibration frequency for all test models. The *RMS* maximum power generation was less than 1.0 mW at designed flow velocity except for $D = 0.3H$. However, Wang and Yuan (2008) found that 0.576mW electric power was sufficient to energize the ultra-capacitor of the wireless sensor. Orrego *et al*. (2017) showed fluttering piezoelectric with ambient wind velocity successfully powered a sensor without a battery.

The bladeless power generator lit 54 *LED* ball lamps at a flow velocity of 3.25 m/s using the rectangular prism with depth, $D = 0.2H$, and span length of 300 mm as the *WRU* with the electric power generated was ≈ 1.4 mW (Fig. 17). The generator's power output is the prospective resource for a remote sensor, wearable, or wireless devices without dependency on the conventional power supply.

The power generation experiment in the wind tunnel test encountered constraints such as one-dimensional wind direction and high displacement of long-span wind receiving unit. These challenges could be unveiled in the initial field test performed to ensure the generator worked well in environmental conditions, as shown in Fig. 17. The moveable wind rudder directed *WRU* to vibrate well with onset vibration of less than 1.0 m/s, working to wind velocity of around 3.5 m/s. The *WRU* displacement and voltage output magnitude were not recorded, but the voltage output signal could be observed at the data acquisition display. Ordonez and Duke (2021) also showed reliability of the bladeless power generator model in field test. The initial field test of the bladeless power generator model recommends future studies to develop a microgrid of power generation from *FIV*.

4. Conclusions

The performance of magnetostrictive material for the micropower generator from *FIV* was performed experimentally in the wind tunnel. The findings showed that the span-length and depth variations of the rectangular prism affect onset galloping, frequency response, and voltage output of the micro-generator. Increasing the *WRU*'s span length reduces the vibration response frequency, *RMS* voltage output, and generator performance. However, it enables the generator to generate a voltage at low wind velocity. Span length variation does not change vibration behavior, such as response range and onset galloping of resonance reduced-velocity V_r for rectangular with $D \leq 0.5H$ and circular cylinder.

The vibration response range of the rectangular prisms with $D/H \leq 0.4$ is smaller than the circular cylinder, which experienced an abrupt down at high wind velocity for span length $L = 300$ and 400 mm. However, this did not occur at prism with a length of 200 mm at the designed flow velocity range. Continuous vibration response was observed at the prism with depth $D \geq 0.5H$ for all span lengths. The micro-generators voltage output is influenced by the displacement rate and frequency response of the *WRU*. However, excessive displacement of *WRU* detaches the bonding harvester from the frame, decreasing the generator performance. Therefore, an abrupt down of *WRU*'s vibration response characteristic at high flow velocity prevents the generator from malfunctioning.

The rectangular prism with depth $D \leq 0.4H$ and span length $L = 7.5H$ is prospective *WRU* for vibration-based power generation. The prominent features of these *WRU* models are downtick vibration at flow velocity less than 5 m/s, low onset galloping against flow velocity, and moderate power output. Furthermore, the generator model's performance suggests that the harvester model could be a power resource for wearable and wireless devices, sensors, and *IoT* systems. The power harvester model from magnetostrictive material also has potential development for moderate scale power output in the future by improving *WRU*'s core size and vibration response characteristics.

Acknowledgement

This work is a part of collaborative work supported by the Ministry of Education, Culture, Sports, Science, and Technology JAPAN through the Program for Building Regional Innovation Ecosystems. The first author is grateful to Mr. Kuratani Tomohiro for his valuable supports in the experimental activities at Fluid Dynamics Laboratory, Kanazawa University JAPAN.

Author Contributions: L.O.A.B.: Conceptualization, methodology, formal analysis, writing—original draft, T.K.; supervision, resources, project administration, T.U.; preparing the micro generator, S; review and editing, project administration. L.H: supervising, proof reading. All authors have read and agreed to the published version of the manuscript.

Funding: This research was funded by Ministry of Education, Culture, Sports, Science, and Technology JAPAN through the Program for Building Regional Innovation Ecosystems.

Conflicts of Interest: The authors declare no conflict of interest.

References

Abdelkefi, A., 2016. Aeroelastic energy harvesting: A review. Int. J. Eng. Sci. 100, 112–135. https://doi.org/10.1016/j.ijengsci.2015.10.006

Abdelkefi, A., Hajj, M.R., Nayfeh, A.H., 2012. Power harvesting from transverse galloping of square cylinder. Nonlinear Dyn. 70, 1355–1363. https://doi.org/10.1007/s11071-012-0538-4

Ahmed, R., Mir, F., Banerjee, S., 2017. A review on energy harvesting approaches for renewable energies from ambient vibrations and acoustic waves using piezoelectricity. Smart Mater. Struct. 26, 085031. https://doi.org/10.1088/1361-665x/aa7bfb

Alrashdan, M.H.S., Hamzah, A.A., Majlis, B.Y., 2015. Design and optimization of cantilever based piezoelectric micro power generator for cardiac pacemaker. Microsyst. Technol. 21, 1607–1617. https://doi.org/10.1007/s00542-014-2334-1

Ansari, M.H., Karami, M.A., 2015. Piezoelectric energy harvesting from heartbeat vibrations for leadless pacemakers. J. Phys. Conf. Ser. 660, 012121. https://doi.org/10.1088/1742-6596/660/1/012121

Anton, S.R., Sodano, H.A., 2007. A review of power harvesting using piezoelectric materials (2003–2006). Smart Mater. Struct. 16, R1–R21. https://doi.org/10.1088/0964-1726/16/3/R01

Apicella, V., Clemente, C.S., Davino, D., Leone, D., Visone, C., 2019. Magneto-mechanical optimization and analysis of a magnetostrictive cantilever beam for energy harvesting. J. Magn. Magn. Mater. 475, 401–407. https://doi.org/10.1016/j.jmmm.2018.11.076

Barata,L.O.A, Kiwata, T., Kono, T., Ueno, T., 2020. Effects of Span Length and Additional Structure on Flow-Induced Transverse Vibration Characteristic of a Cantilevered Rectangular Prism. J. Flow Control. Meas. Vis. 08, 102–120. https://doi.org/10.4236/jfcmv.2020.83006

Bearman, P.W., 2011. Circular cylinder wakes and vortex-induced vibrations. J. Fluids Struct. 27, 648–658. https://doi.org/10.1016/j.jfluidstructs.2011.03.021

Bearman, P.W., 1984. VORTEX SHEDDING FROM OSCILLATING BLUFF BODIES. Annu. Rev. Fluid Mech. 16, 195–222.

Bernitsas, M.M., Raghavan, K., Ben-Simon, Y., Garcia, E.M.H., 2008. VIVACE (Vortex Induced Vibration Aquatic Clean Energy): A New Concept in Generation of Clean and Renewable Energy From Fluid Flow. J. Offshore Mech. Arct. Eng. 130, 1–15. https://doi.org/10.1115/1.2957913

Betz, A., 1966. Introduction to Theory of Flow Machine. Pergamon Press, Oxford.

Blevins, R.D., 1974. Flow induced Vibrations of Bluff Structures. California Institute of Technology.

Derakhshandeh, J.F., Arjomandi, M., Cazzolato, B.S., Dally, B., 2015. Harnessing hydro-kinetic energy from wake-induced vibration using virtual mass spring damper system. Ocean Eng. 108, 115–128. https://doi.org/10.1016/j.oceaneng.2015.08.003

Edward Romero-Ramirez, 2010. Energy harvesting from body motion using rotational micro- generation. Michigan Technological University.

Gonçalves, R.T., Rosetti, G.F., Franzini, G.R., Meneghini, J.R., Fujarraa, A.L.C., 2013. Two-degree-of-freedom vortex-induced vibration of circular cylinders with very low aspect ratio and small mass ratio. J. Fluids Struct. 39. https://doi.org/10.1016/j.jfluidstructs.2013.02.004

Jafari, H., Ghodsi, A., Azizi, S., Ghazavi, M.R., 2017. Energy harvesting based on magnetostriction, for low frequency excitations. Energy 124, 1–8. https://doi.org/10.1016/j.energy.2017.02.014

Kiwata, T., Yamaguchi, M., Kono, T., Ueno, T., 2014. Water tunnel experiments on transverse-galloping of cantilevered rectangular and D-section prisms. J. Fluid Sci. Technol. 9, 1–11. https://doi.org/10.1299/jfst.2014jfst00

Liu, Cong, Zhao, Ma, 2019. Comprehensive Analysis of the Energy Harvesting Performance of a Fe-Ga Based Cantilever Harvester in Free Excitation and Base Excitation Mode. Sensors 19, 3412. https://doi.org/10.3390/s19153412

Liu, H., Cong, C., Cao, C., Zhao, Q., 2020. Analysis of the Key Factors Affecting the Capability and Optimization for Magnetostrictive Iron-Gallium Alloy Ambient Vibration Harvesters. Sensors 20, 401. https://doi.org/10.3390/s20020401

Matsuzaki, R., Todoroki, A., 2008. Wireless Monitoring of Automobile Tires for Intelligent Tires. Sensors 8, 8123–8138. https://doi.org/10.3390/s8128123

Mitcheson, P.D., Miao, P., Stark, B.H., Yeatman, E.M., Holmes, A.S., Green, T.C., 2004. MEMS electrostatic micropower generator for low frequency operation. Sensors Actuators A Phys. 115, 523–529. https://doi.org/10.1016/j.sna.2004.04.026

Mizota, T., Okajima, A., 1992. Unsteady aerodynamic forces and wakes of rectangular prisms with oscillating flaps at leading edges. J. Wind Eng. Ind. Aerodyn. 41, 727–738. https://doi.org/10.1016/0167-6105(92)90489-W

Mizukami, S., Kiwata, T., Kono, T., Barata, L.O., Ueno, T., 2017. Transverse Vibration Characteristics of a Rectangular Prism with Small Side Ratio and Flow Field around the Prism:-Effect of Having and not Having an End of the Prism (In Japanese). Proc. Mech. Eng. Congr. Japan 2017S05205, 1–6. https://doi.org/https://doi.org/10.1299/jsmemecj.2017.S0520506

Mohammadi, S., Esfandiari, A., 2015. Magnetostrictive vibration energy harvesting using strain energy method. Energy 81, 519–525. https://doi.org/10.1016/j.energy.2014.12.065.

Mohanty, A., Parida, S., Behera, R.K., Roy, T., 2019. Vibration energy harvesting: A review. J. Adv. Dielectr. 09, 1930001. https://doi.org/10.1142/S2010135X19300019

Nakaguchi, H., Hashimoto K., & Muto, S. (1968). An Experimental Study on Aerodynamic Drag of Rectangular Cylinders. The Journal of the Japan Society of Aeronautical Engineering, 16(168), 1–5. https://doi.org/10.2322/jjsass1953.16.1

Nakamura, Y., Hirata, K., 1989. Critical geometry of oscillating bluff bodies. J. Fluid Mech. 208, 375–393. https://doi.org/10.1017/S0022112089002879.

Nakamura, Y., Hirata, K., 1991. Pressure fluctuations on oscillating rectangular cylinders with the long side normal to the flow. J. Fluids Struct. 5, 165–183. https://doi.org/10.1016/0889-9746(91)90460-7.

Nakamura, Y., Matsukawa, T., 1987. Vortex excitation of rectangular cylinders with a long side normal to the flow. J. Fluid Mech. 180, 171. https://doi.org/10.1017/S0022112087001770.

Narita, F., Fox, M., 2018. A Review on Piezoelectric, Magnetostrictive, and Magnetoelectric Materials and Device Technologies for Energy Harvesting Applications. Adv. Eng. Mater. 20, 1–22. https://doi.org/10.1002/adem.201700743.

Ohya, Y., 1994. Note on a discontinuous change in wake pattern for a rectangular cylinder. J. Fluids Struct. 8, 325–330.

Okajima, A., Kiwata, T., 2019. Flow-Induced Stream-Wise Vibration of Circular Cylinders. J. Flow Control. Meas. & Vis. 07, 133–151. https://doi.org/10.4236/jfcmv.2019.73011.

Okajima, A., Matsumoto, T., Kimura, S., 2000. Flow characteristics of a rectangular cylinder with a cross-section of various width/height ratios submerged in oscillatory flow. JSME Int. J. Ser. B-Fluids Therm. Eng. 43, 329–338.

Okajima,A., Kimura,S., Katayama,T., Ohtsuyama,S. and Ojima,A., (1998). Fluid-dynamic characteristics of a rectangular cylinder with various width-to-ratios in wide range of Reynolds number. Journal of Structural Engineering, Vol.44A, pp.971-977 (in Japanese).

Ordoñez, O., & Duke, A. R. (2021). Wind Resource Assessment : Analysis of the Vortex Bladeless Characteristics in Puerto Cortés , Honduras Wind Resource Assessment : Analysis of the Vortex Bladeless Characteristics in Puerto Corté s , Honduras, 801(2021), 1–8. https://doi.org/10.1088/1755-1315/801/1/012019

Orrego, S., Shoele, K., Ruas, A., Doran, K., Caggiano, B., Mittal, R., & Hoon, S. (2017). Harvesting ambient wind energy with an inverted piezoelectric flag. Applied Energy, 194, 212–222. https://doi.org/10.1016/j.apenergy.2017.03.016

Palau-Salvador, G., Stoesser, T., Fröhlich, J., Kappler, M., Rodi, W., 2010. Large eddy simulations and experiments of flow around finite-height cylinders, Flow, Turbulence and Combustion. https://doi.org/10.1007/s10494-009-9232-0.

Poloni, T., Lu, J., 2017. An Indirect Tire Health Monitoring System Using On-board Motion Sensors. SAE Tech. Pap. 2017-March. https://doi.org/10.4271/2017-01-1626.

Rostamy, N., Sumner, D., Bergstrom, D.J., Bugg, J.D., 2012. Local flow field of a surface-mounted finite circular cylinder. J. Fluids Struct. 34, 105–122. https://doi.org/10.1016/j.jfluidstructs.2012.04.014

Sakamoto, H., 1985. Aerodynamic forces acting on a rectangular prism placed vertically in a turbulent boundary layer. J. Wind Eng. Ind. Aerodyn. 18, 131–151. https://doi.org/10.1016/0167-6105(85)90093-5.

Sumner, D., Rostamy, N., Bergstrom, D.J., Bugg, J.D., 2017. Influence of aspect ratio on the mean flow field of a surface-mounted finite-height square prism. Int. J. Heat Fluid Flow 65, 1–20. https://doi.org/10.1016/J.IJHEATFLUIDFLOW.2017.02.004.

Ueno, T., Yamada, S., 2011. Performance of energy harvester using iron-gallium alloy in free vibration. IEEE Trans. Magn. 47, 2407–2409. https://doi.org/10.1109/TMAG.2011.2158303.

Wang, J., Gu, S., Zhang, C., Hu, G., Chen, G., Yang, K., Li, H., Lai, Y., Litak, G., Yurchenko, D., 2020. Hybrid wind energy scavenging by coupling vortex-induced vibrations and galloping. Energy Convers. Manag. 213, 112835. https://doi.org/10.1016/j.enconman.2020.112835.

Wang, L., Yuan, F.G., 2008. Vibration energy harvesting by magnetostrictive material. Smart Mater. Struct. 17. https://doi.org/10.1088/0964-1726/17/4/045009.

Wang, H.F., Zhou, Y., 2009. The finite-length square cylinder near wake. J. Fluid Mech. 638, 453–490. https://doi.org/10.1017/S0022112009990693.

Williamson, C.H.K., Govardhan, R., 2004. Vortex-Induced Vibrations. Annu. Rev. Fluid Mech. 36, 413–455. https://doi.org/10.1146/annurev.fluid.36.050802.122128.

Yan, B., Zhang, C., Li, L., 2018. Magnetostrictive energy generator for harvesting the rotation of human knee joint. AIP Adv. 8, 056730. https://doi.org/10.1063/1.5007195.

Zdravkovich, M.M., 1981. Review and classification of various aerodynamic and hydrodynamic means for suppressing vortex shedding. J. Wind Eng. Ind. Aerodyn. 7, 145–189. https://doi.org/10.1016/0167-6105(81)90036-2.

Zhong, W., Deng, L., Xiao, Z., 2019. Flow past a rectangular cylinder close to a free surface. Ocean Eng. 186, 106118. https://doi.org/10.1016/j.oceaneng.2019.106118